

# Human Protein-disulfide Isomerase Is a Redox-regulated Chaperone Activated by Oxidation of Domain a'\*

Received for publication, September 10, 2011, and in revised form, October 24, 2011. Published, JBC Papers in Press, November 16, 2011, DOI 10.1074/jbc.M111.303149

Chao Wang<sup>§1</sup>, Jiang Yu<sup>¶1,2</sup>, Lin Huo<sup>‡</sup>, Lei Wang<sup>‡</sup>, Wei Feng<sup>‡3</sup>, and Chih-chen Wang<sup>‡4</sup>

From the <sup>‡</sup>National Laboratory of Biomacromolecules, Institute of Biophysics, Chinese Academy of Sciences, Beijing 100101, China, the <sup>§</sup>Graduate University of the Chinese Academy of Sciences, Beijing 100049, China, and the <sup>¶</sup>Division of Life Sciences, Molecular Neuroscience Center, State Key Laboratory of Molecular Neuroscience, Hong Kong University of Science and Technology, Clear Water Bay, Kowloon, Hong Kong, China

**Background:** Human protein-disulfide isomerase (hPDI) is a key enzyme and chaperone for protein folding.

**Results:** Oxidation of domain a' releases the compact conformation of hPDI and exposes the buried substrate-binding sites facilitating its high chaperone activity.

**Conclusion:** Oxidation of hPDI activates its chaperone activity.

**Significance:** This study provides the first structural evidence of and mechanistic insights into the redox-regulated chaperone activity of hPDI.

Protein-disulfide isomerase (PDI), with domains arranged as  $abb'xa'c$ , is a key enzyme and chaperone localized in the endoplasmic reticulum (ER) catalyzing oxidative folding and preventing misfolding/aggregation of proteins. It has been controversial whether the chaperone activity of PDI is redox-regulated, and the molecular basis is unclear. Here, we show that both the chaperone activity and the overall conformation of human PDI are redox-regulated. We further demonstrate that the conformational changes are triggered by the active site of domain a', and the minimum redox-regulated cassette is located in  $b'xa'$ . The structure of the reduced  $bb'xa'$  reveals for the first time that domain a' packs tightly with both domain b' and linker x to form one compact structural module. Oxidation of domain a' releases the compact conformation and exposes the shielded hydrophobic areas to facilitate its high chaperone activity. Thus, the study unequivocally provides mechanistic insights into the redox-regulated chaperone activity of human PDI.

the folding and maturation of membrane and secretory proteins (1). PDI is a key enzyme (2) and chaperone (3, 4) localized in the ER with versatile functions (*e.g.* catalyzing formation, breakage, and rearrangement of the disulfide bonds in protein substrates (5), facilitating ER-associated degradation of misfolded proteins (6, 7), and serving as a chaperone-like subunit of prolyl-4-hydroxylase (8) and microsomal triglyceride transfer protein (9)). Additionally, PDI has non-ER locations (10); for example, on the cell surface, it participates in the activation of the fusion of HIV virus (11) and mediates the adhesion, secretion, and aggregation of platelet (12). Recently, it has been recognized that PDI plays a critical role in the control of neurodegenerative diseases related to protein misfolding and aggregation (*e.g.* Alzheimer disease, Parkinson disease, amyotrophic lateral sclerosis, and Huntington disease (13–16)).

PDI is composed of four thioredoxin-like domains (a, b, b', and a') plus an x linker and a C-terminal acidic tail (Fig. 1A) (17–19). Both domains of a and a' contain a CGHC active site responsible for the oxidoreductase activity (20). The b' domain possesses the main peptide binding site, whereas binding of large substrates or partner proteins requires all four domains (21, 22). The crystal structures of yeast PDI (yPDI) at 4 and 22 °C revealed that four domains are arranged in a “twisted U shape” and a “boat shape,” respectively, with domains a and a' representing two mobile arms connected to the rigid bb' base, and the a arm was demonstrated to be more flexible than the a' arm (23, 24). The full-length structure of hPDI has not been reported so far; however, the major flexible sites are located in the b'xa' region (25). PDI can shuttle between the oxidized and reduced states with abilities to bind to various targets and catalyze different reactions (*i.e.* the oxidized PDI preferentially binds to reduced/unfolded polypeptide to introduce disulfide bonds, whereas the reduced PDI mainly interacts with misoxidized substrates functioning as a reductase or isomerase (26)). In mammalian cells, only the reduced and not the oxidized PDI interacts with its oxidase Ero1 (27) or peroxiredoxin 4 (28). Hence, it is elusive how reduced/oxidized PDI distinguishes its

The ER<sup>5</sup> is a eukaryotic organelle containing many chaperones and enzymes and provides an optimized environment for

\* This work was supported by National Major Basic Research Program of China Grants 2011CB910303 and 2011CB910503, National Natural Science Foundation of China Grants 31000351 and 31070657, and Knowledge Innovation Program of the Chinese Academy of Sciences Grants KSCX2-YW-R-154 and KSCX2-EW-J-3.

§ This article contains supplemental Table S1 and Figs. S1–S3.

The atomic coordinates and structure factors (code 3UEM) have been deposited in the Protein Data Bank, Research Collaboratory for Structural Bioinformatics, Rutgers University, New Brunswick, NJ (<http://www.rcsb.org/>).

<sup>1</sup> Both authors contributed equally to this work.

<sup>2</sup> Present addresses: School of Physics, University of New South Wales, Sydney, New South Wales 2052, Australia and the Centre for Applied Medical Research, St Vincent's Hospital, Sydney, New South Wales 2010, Australia.

<sup>3</sup> To whom correspondence may be addressed. Tel.: 86-10-64888751; Fax: 86-10-64888237; E-mail: wfeng@ibp.ac.cn.

<sup>4</sup> To whom correspondence may be addressed. Tel.: 86-10-64888500; Fax: 86-10-64840672; E-mail: chihwang@sun5.ibp.ac.cn.

<sup>5</sup> The abbreviations used are: ER, endoplasmic reticulum; PDI, protein-disulfide isomerase; hPDI, human PDI; yPDI, yeast PDI; ANS, 1-anilino-8-naphthalene sulfonate.

## Oxidation of hPDI Activates Its Chaperone Activity

substrates/partner proteins or selectively binds to the same substrate at different stages in the protein-folding pathway (26).

About 10 years ago, PDI was reported to be a redox-dependent chaperone based on the finding that PDI binds and unfolds the cholera toxin A1 subunit in the reduced form (29) and releases it after being oxidized by Ero1, thus facilitating the retrograde transport of A1 subunit from the ER into the cytosol (30). However, this redox-dependent chaperone activity of PDI was subsequently challenged by arguing that the release of the A1 subunit is mediated by substrate competition rather than by a change in the redox state of PDI (31). Therefore, whether the chaperone activity of PDI is redox-regulated is controversial (32). Moreover, the putative redox-dependent conformational changes of PDI are much less characterized, and only very recently, studies of PDI from a thermophilic fungus showed a redox-dependent intramolecular rearrangement of the **b'** and **a'** domains by using NMR spectroscopy and small-angle x-ray scattering (33, 34). Nevertheless, the underlying molecular mechanism for redox-regulated conformational changes and chaperone activity of PDI remains largely unknown.

In this study, we extensively explored different conformations and the chaperone activity of hPDI in different redox states. We demonstrate that hPDI is a redox-regulated chaperone undergoing large redox-dependent conformational changes. We further map out **b'xa'** to be the minimal region of hPDI enduring the conformational rearrangement and identify the active site in the **a'** domain to be the key trigger. The crystal structure of the reduced **bb'xa'** was determined and reveals that the **a'** domain packs tightly with both the **b'** domain and the **x** linker to form one compact structural module. Oxidation of the **a'** domain releases this compact conformation and subsequently exposes the shielded substrate binding areas for higher chaperone activity of hPDI. We finally demonstrate that the redox-dependent conformational changes are essential for regulation of the chaperone activity of hPDI.

### EXPERIMENTAL PROCEDURES

**Plasmid Construction and Protein Purification**—The genes encoding hPDI, **abb'x** and **bb'xa'**, were cloned into pQE30 (Qiagen), and the resulting proteins contained N-terminal (MRGSH<sub>6</sub>GS) tags. The **bb'xa'** gene was also cloned into a modified pET32a for structural studies, and the resulting protein contained an N-terminal (H<sub>6</sub>SSGLEVLVFGQSEF) tag. hPDI mutants were created by the overlap extension PCR method, and the sequences of all of the constructs were verified by DNA sequencing. Proteins were expressed and purified as described previously (35). Protein concentrations were determined by the Bradford method with bovine serum albumin as a standard.

**Chaperone Activity**—Complete denaturation of glyceraldehyde-3-phosphate dehydrogenase (GAPDH) was carried out by incubation of 0.14 mM GAPDH in 3 M guanidine hydrochloride with 1 mM DTT overnight at 4 °C. Refolding was initiated by 50-fold dilution of the denatured GAPDH into 100 mM sodium phosphate buffer (pH 7.4) containing 2.5 mM EDTA in the absence or presence of hPDI proteins and different concentrations of DTT at 25 °C. Aggregation produced during the refolding was monitored by recording the light scattering at 488 nm,

and the suppression of aggregation was used to measure the chaperone activity of hPDI proteins (3).

**Limited Proteolysis Assay**—hPDI proteins at 1 mg/ml were incubated with or without 1 mM GSH, GSSG, or DTT in 50 mM Tris-HCl buffer (pH 7.6) containing 5 mM CaCl<sub>2</sub> at 25 °C for 30 min, and then different proteases were added for digestion. The reactions were terminated at different times by phenylmethanesulfonyl fluoride (PMSF) and analyzed by reducing SDS-PAGE.

**Fluorescence Measurements**—hPDI proteins of 5 μM were incubated with or without 1 mM GSH, GSSG, or DTT in 50 mM Tris-HCl buffer (pH 7.6) containing 150 mM NaCl at 25 °C for 30 min. Intrinsic fluorescence spectra were recorded at 310–400 nm at 25 °C with excitation at 290 nm. 1-Anilino-8-naphthalene sulfonate (ANS) was added in protein samples to 50 μM and incubated for 20 min at 25 °C in the dark before the ANS fluorescence emission spectra (400–600 nm) were determined with excitation at 370 nm. The concentration of ANS was determined using an extinction coefficient at 350 nm of 5000 M<sup>-1</sup> cm<sup>-1</sup>.

**Crystallization, Data Collection, and Process**—The purified **bb'xa'** at 10.0 mg/ml in 20 mM Tris-HCl buffer, 100 mM NaCl, pH 7.5, was crystallized at 16 °C using the hanging drop method by mixing 1 μl of protein sample containing 50 mM DTT with an equal volume of 25% (w/v) PEG 3350 in 0.1 M Tris-HCl, 0.2 M ammonium acetate, pH 8.5. The crystals were flash-cooled with liquid nitrogen. The diffraction data were collected at Shanghai Synchrotron Radiation Facility beam line BL17U at a wavelength of 0.979 Å at 100 K. The diffraction data were processed and scaled using HKL2000 package (36).

**Structure Determination and Refinement**—The **bb'xa'** structure was solved by the molecular replacement method with the program Phaser (37) using the structure of yPDI (Protein Data Bank code 2B5E) (23) as the search model. Structures were fitted and rebuilt with the program Coot (38) and refined with REFMAC5 (37) and CNS (40). At the final refinement stage, TLS refinement was used with groups defined by the TLSMD server (41). The overall quality of the final structural model was assessed by PROCHECK (42). The atomic coordinates of **bb'xa'** have been deposited in the Protein Data Bank (PDB code 3UEM).

**Mass Spectrometry**—Protein samples were purified by size exclusion chromatography with 0.1% formic acid/water for digests by proteinase K and by reverse-phase HPLC on a C8 chip (G4240-63001) with a water-ACN system containing 0.1% formic acid for digests by trypsin or chymotrypsin. The samples were introduced into the spectrometer by JetStream electrospray ionization using a spray voltage of 3.7 kV for digests by proteinase K and by HPLC-chip using 1.88 kV for digests by trypsin or chymotrypsin. Spectra were acquired on a calibrated Q-TOF (Agilent 6530) instrument operated in positive ion mode over the *m/z* range 400–1600 for digests by proteinase K and 400–3200 for digests by trypsin or chymotrypsin. Data were processed via Mass Hunter qualitative analysis software.

### RESULTS

**Chaperone Activity of hPDI Is Regulated by Its Redox States**—To reconcile the controversy on redox-regulated chaperone

## Oxidation of hPDI Activates Its Chaperone Activity

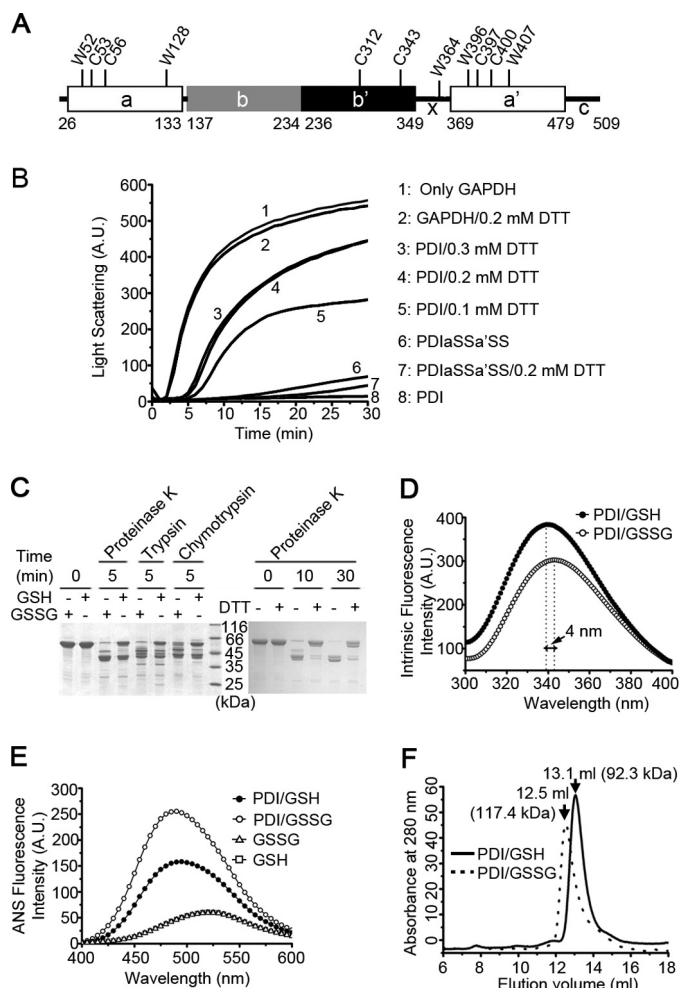


**FIGURE 1. The chaperone activity and overall conformation of hPDI are redox-regulated.** *A*, a schematic representation of hPDI with domain organization in **abb'xa'c**. The positions of all of the tryptophan and cysteine residues are marked, and the residue numbering is for hPDI with signal sequence. *B*, hPDI is a redox-regulated chaperone. Guanidine hydrochloride-denatured GAPDH at 0.14 mM was 50-fold diluted into refolding buffer in the absence or presence of 28  $\mu$ M hPDI proteins with various concentrations of DTT as indicated. Aggregation produced during the refolding was monitored by recording the light scattering at 488 nm, and the suppression of aggregation was used to measure the chaperone activity of hPDI proteins. A.U., arbitrary units. *C*, protease digestion profiles of hPDI at different redox states. hPDI at 1 mg/ml was incubated with 1 mM GSSG, GSH, or DTT at 25 °C for 30 min and then digested by 2  $\mu$ g/ml proteinase K, trypsin, or chymotrypsin for various time as indicated. The reactions were terminated by adding PMSF to a final concentration of 0.5 mM and analyzed by reducing SDS-PAGE. The oxidized hPDI is more accessible for protease digestion than the reduced hPDI. *D* and *E*, fluorescence spectra of hPDI at different redox states. hPDI at 5  $\mu$ M was incubated with 1 mM GSSG or GSH at 25 °C for 30 min, and the intrinsic (*D*) and ANS (*E*) fluorescence spectra were recorded. A.U., arbitrary units. *F*, size exclusion chromatography profiles of hPDI treated with 1 mM GSH (solid curve) or GSSG (dashed curve) at 25 °C for 30 min. The molecular weight of hPDI in different redox states calculated according to the elution volume is marked.

activity of hPDI, we first tested whether the chaperone activity of hPDI is regulated by its redox states. A well established system was used to characterize the chaperone activity of hPDI (3) (*i.e.* the presence of hPDI in the refolding buffer strongly suppressed the aggregation of guanidine hydrochloride-denatured GAPDH during dilution-induced refolding) (Fig. 1*B*). The purified hPDI contains about 2.5 free thiols as determined by 5,5'-dithiobis(2-nitrobenzoic acid), indicating the active sites in

domains **a** and **a'** are mostly oxidized because the two cysteines in the **b'** domain do not form a disulfide bond (43). Adding DTT in the refolding buffer significantly decreased the chaperone activity of hPDI in a concentration-dependent manner (*i.e.* the more reduced hPDI was, the lower chaperone activity it showed) (Fig. 1*B*), demonstrating that the redox states of hPDI indeed control its chaperone activity. Because both active sites of domains **a** and **a'** are redox state sensors, we next made double Cys/Ser point mutations on both sites (PDIaSSa'SS) to impair its redox responses. Notably, PDIaSSa'SS showed chaperone activity similar to that of the oxidized hPDI, and the DTT-induced chaperone activity decrease was completely abolished (Fig. 1*B*), indicating that redox-regulated hPDI chaperone activity is dependent on its active sites.

*hPDI Undergoes Redox-dependent Conformational Changes*—We next looked for the potential redox-dependent conformational changes of hPDI by direct digestion with proteinase K, trypsin, and chymotrypsin under various redox conditions (Fig. 1*C*). After 5 min of digestion by proteinase K, the GSSG-incubated hPDI almost disappeared, whereas about half of the GSH-incubated hPDI was intact. Similar digestion profiles were produced by trypsin and chymotrypsin. To avoid S-glutathionylation-induced conformational change, hPDI was next digested in the presence or absence of DTT. After a 10-min digestion by proteinase K, most of hPDI but little of the DTT-incubated hPDI was digested (Fig. 1*C*). Hence, the oxidized hPDI adopts a loose conformation, and the reduced one is very compact.

We next carried out fluorescence studies of hPDI under different redox conditions to further probe redox-regulated conformational changes. Consistent with a compact conformation of the reduced hPDI, the intrinsic fluorescence spectrum of the GSH-incubated hPDI showed a blue shift ( $\sim$ 4 nm) of the maximum excited wavelength compared with that of the GSSG-incubated hPDI (Fig. 1*D*). The GSSG-incubated hPDI showed higher ANS fluorescence intensity than that of the GSH-incubated hPDI, again indicating the oxidized hPDI being much looser and exposing more hydrophobic areas (Fig. 1*E*). Additionally, the intrinsic and ANS fluorescence spectra of DTT-treated and -untreated hPDI showed similar results (supplemental Fig. S1). Finally, size exclusion chromatography analysis also demonstrated that the reduced hPDI was eluted with a larger volume, confirming its compact conformation (Fig. 1*F*). Taken together, hPDI shows significant conformational changes induced by different redox conditions.

*Redox States of a' Domain Regulate Interdomain Conformations of b'xa'*—To identify the critical cysteine responsible for the redox-regulated conformational changes of hPDI, we made cysteine mutations in **a**, **b'**, or **a'** domain, respectively. The digestion profiles of the mutants (Fig. 2*A*) showed that the redox-regulated susceptibility to hydrolysis disappeared only for the **a'** domain mutant (PDIaCCa'SS), indicating that the active site of the **a'** domain is the key position. Moreover, mutation of either cysteine in the **a'** domain resulted in loss of the redox-regulated conformational changes (supplemental Fig. S2). Furthermore, the protease digestion profiles (Fig. 2*B*) and the intrinsic (Fig. 2*C*) and ANS (Fig. 2*D*) fluorescence spectra of **abb'x** and **bb'xa'** in different redox conditions were deter-



**TABLE 1**  
Data collection and refinement statistics

<b>Diffraction data</b>	
Space group	P2 <sub>1</sub> 2 <sub>1</sub> 2 <sub>1</sub>
Unit cell (Å)	<i>a</i> = 63.585, <i>b</i> = 76.076, <i>c</i> = 79.656, α = β = γ = 90°
Resolution (Å)	50–2.29 (2.38–2.29) <sup>a</sup>
Unique reflections	17,802
<i>R</i> <sub>merge</sub> <sup>b</sup> (%)	4.7 (41.2)
<i>I</i> / <i>σ</i>	30.3 (3.9)
Average redundancy	5.1 (5.3)
Completeness (%)	99.5 (100.0)
<b>Refinement</b>	
Resolution (Å)	50–2.29 (2.35–2.29)
<i>R</i> <sub>work</sub> <sup>c</sup> (last shell)	22.3 (30.9)
<i>R</i> <sub>free</sub> <sup>d</sup> (last shell)	28.0 (39.2)
Mean <i>B</i> factors (Å <sup>2</sup> )	55.4
Bond length <sup>e</sup> (Å)	0.007
Bond angles (degrees)	1.044
Ramachandran plot (residues, %)	
Most favored	93.0
Additionally allowed	6.6
Generously allowed	0.3

<sup>a</sup> The values in parentheses refer to the highest resolution shell.

<sup>b</sup>  $R_{\text{merge}} = \frac{\sum_h \sum_l |I_h|}{\sum_h \sum_l I_h}$ , where  $I_h$  is the mean intensity of the  $h$  observation of reflection  $h$ .

<sup>c</sup>  $R_{\text{factor}} = \frac{\sum_h ||F_o| - |F_c||}{\sum_h |F_o|}$ , where  $|F_o|$  and  $|F_c|$  are the observed and calculated structure factor amplitudes, respectively. Summation includes all reflections used in the refinement.

<sup>d</sup>  $R_{\text{free}} = \frac{\sum ||F_o| - |F_c||}{\sum |F_o|}$ , evaluated for a randomly chosen subset of 5% of the diffraction data not included in the refinement.

<sup>e</sup> Root mean square deviation from ideal values.

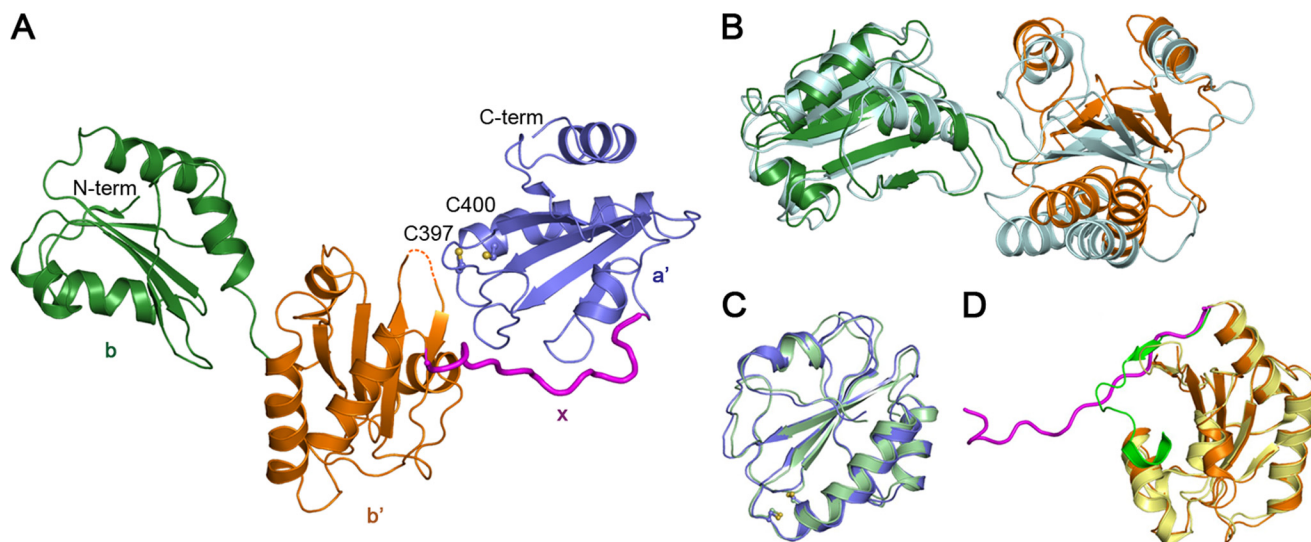


**FIGURE 3. Overall structure of the reduced  $bb'xa'$ .** *A*, a ribbon diagram of the crystal structure of the reduced  $bb'xa'$ . The **b**, **b'**, **x**, and **a'** domains are colored in green, orange, magenta, and blue, respectively. The side chains of the active site cysteines in domain **a'** are shown as sticks. Both the N and C termini are also labeled. *B*, superimposed overlay of the  $bb'$  tandem in the solution structure (44) (cyan) and that in the crystal structure of  $bb'xa'$  based on domain **b**. *C*, superposition of the **a'** domain in the solution structure (Protein Data Bank entry 1X5C) (pale green) and that in the crystal structure of  $bb'xa'$ . *D*, superposition of the crystal structure of 1289A **b'x** (43) (the **b'** domain in yellow and the **x** linker in forest green) and **b'x** in the crystal structure of  $bb'xa'$ .

Lys-326, Met-356–Glu-431, Ser-357–Gly-374 and –Lys-375, Gln-358–Asn-430, Trp-364–Val-371, and Asp-365–Lys-370) (Fig. 4*B*, left). Although the relative positions of domains **b'** and **a'** are different among yPDI, ERp57, and the reduced  $bb'xa'$ , the interaction pattern between the **x** linker and the **b'** or **a'** domain is similar (*i.e.* hydrophobic interactions in the N-terminal **x** linker and intensive hydrogen bonds in the central and C-terminal **x** linker).

Surprisingly, direct interactions between domains **b'** and **a'** were observed in the reduced  $bb'xa'$  (Fig. 4*B*, right), whereas little was found in yPDI<sub>22°C</sub>, yPDI<sub>4°C</sub>, and ERp57. The side chain of Trp-396 in the **a'** domain exists in two alternative conformations; in one, it forms a cation- $\pi$  interaction with the side chain of Arg-300 in the **b'** domain, and in the other, it contacts with Pro-395 and Thr-428. Interestingly, the side

chain of His-438 in the **a'** domain also adopts two alternative conformations with the major conformation, in which it is buried in the hydrophobic pocket formed by Phe-304, Ile-318, Leu-320, and Met-324 in the **b'** domain. In addition, Lys-326 in domain **b'** forms a salt bridge with Glu-431 in domain **a'**, and Phe-304 in domain **b'** interacts with Thr-428, Phe-440, and His-438 in domain **a'** (Fig. 4*B*, right). It is noteworthy that most of residues in the interface of domains **b'** and **a'** (Arg-300, Phe-304, Ile-318, Leu-320, Met-324, Trp-396, Thr-428, His-438, and Phe-440) coincidentally have been previously characterized for ligand binding (34, 43, 44). Therefore, the reduced **a'** domain packs extensively with both the **b'** domain and the **x** linker to form a compact structural module that shields parts of the substrate binding areas, explaining why reduced hPDI has much lower chaperone activity (Fig. 1*B*). To test whether such

## Oxidation of hPDI Activates Its Chaperone Activity

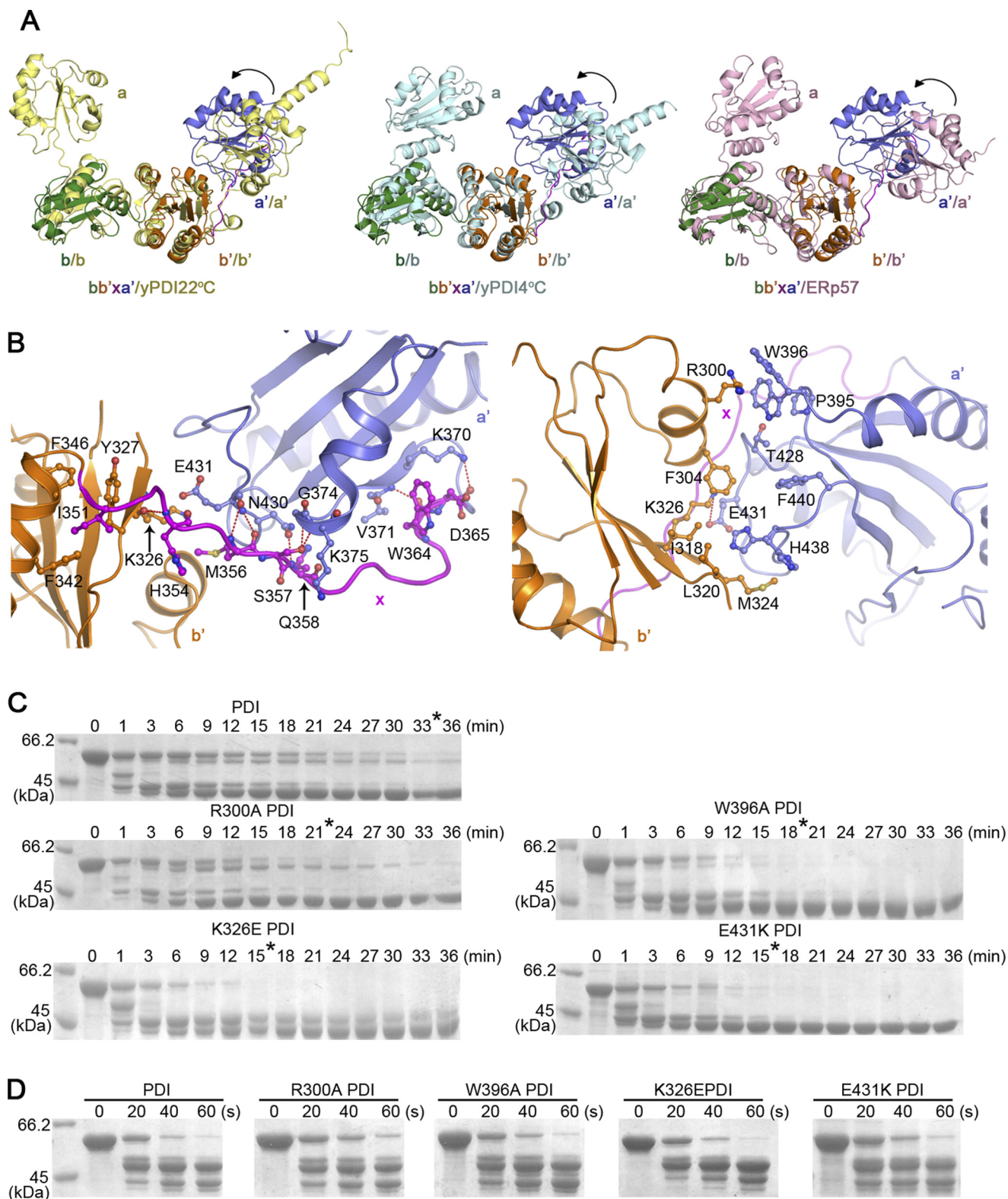


**FIGURE 4. Reduced  $bb'xa'$  adopts a compact conformation.** *A*, superpositions of the reduced  $bb'xa'$  with yPDI structure at 22 °C (24) (yPDI<sub>22°C</sub>) (left) or 4 °C (23) (yPDI<sub>4°C</sub>) (middle) and ERp57 structure (45) (right) based on the  $bb'$  domains. The interdomain motions of the  $a'$  domain relative to the  $bb'$  domains are indicated by arrows. *B*, left, the interface of the  $x'$  linker with domains of  $b'$  and  $a'$ ; right, the interface between domains of  $b'$  and  $a'$ . Residues involved in the interaction are labeled and shown in sticks. Hydrogen bonds (left) and the salt bridge (right) are indicated with red dashed lines. The  $b'$ ,  $x'$ , and  $a'$  are colored in orange, magenta, and blue, respectively. *C* and *D*, protease digestion profiles of hPDI with various point mutations on the interface of the compact  $bb'xa'$  structure. hPDI and the mutants at 1 mg/ml were incubated with 1 mM GSH (*C*) and GSSG (*D*) at 25 °C for 30 min and then digested by 2  $\mu$ g/ml proteinase K for different times as indicated. The reactions were terminated by adding PMSF to a final concentration of 0.5 mM and analyzed by reducing SDS-PAGE. The time for complete digestion of hPDI and its mutants under GSH conditions are indicated by asterisks. All hPDI mutants showed increased accessibility for protease digestion at reduced conditions.

direct interactions between the **b'** and **a'** domains identified in the crystal structure also exist in reduced hPDI in solution, we selectively made R300A, W396A, K326E, and E431K mutants. After incubation with GSH, these mutants are more susceptible to proteinase K than wild-type PDI (Fig. 4C). As the control, the mutants and wild-type PDI showed similar susceptibility to protease digestion after incubation with GSSG (Fig. 4D). These results indicated that the interdomain interactions in **b'xa'** stabilize the compact conformation of the reduced hPDI.

**Oxidation of Active Site in a' Domain Exposes Shielded Interfaces**—To further understand how oxidation of the **a'** domain opens the compact conformation of hPDI, we next tried to identify oxidation-induced exposed regions in detail. The SDS-polyacrylamide gel mobility analysis showed that the major digested products (indicated by *asterisks*) of proteinase K, trypsin, or chymotrypsin are largely comparable but with different intensity between the oxidized and reduced hPDI, indicating that the major digestion sites are similar and more exposed in the oxidized form (supplemental Fig. S3A). These digests were then further analyzed by mass spectrometry (Fig. 5A). Our previous work has shown that the C-terminal half of hPDI is more flexible to be digested than the N-terminal half (25). Indeed, all of the observed molecular mass of major products corresponds to the fragment extending from the N-terminal tag to a residue in the **a'** domain (supplemental Table S1). Although three proteases have different preferences for attacking amino acid residues, they target similar regions in the oxidized hPDI, including the beginning part (Lys-370, Leu-372, and Lys-375), a region around the active sites (Ala-394, Trp-396, and Lys-401), the  $\beta$ 2 sheet (Ala-423, Lys-424, Met-425, and Asp-426), and the  $\beta$ 2- $\beta$ 3 loop (Thr-428 and His-438) of the **a'** domain (Fig. 5B). However, the corresponding products in the mass spectra of the reduced hPDI are either in very low intensity or not observed (Fig. 5A), indicating that these residues are protected from digestion. Interestingly, most of them are located at the interfaces between domains **b'** and **a'** (Ala-394, Trp-396, Thr-428, and His-438) or between domain **a'** and the **x** linker (Lys-370 and Lys-375). Hence, the mass spectrometry analysis firmly demonstrated that the oxidation of the active site in the **a'** domain releases the compact module formed by domains **b'**, **a'**, and the **x** linker and exposes shielded sites for digestion.

**Conformational Transfer Is Essential for Redox-regulated hPDI Chaperone Activity**—As indicated above, significant interdomain conformational changes of hPDI occur in response to different redox conditions. We envision that this kind of compact/loose conformation transfer could directly regulate hPDI chaperone activity by shielding/exposing the substrate binding areas. We next tested the chaperone activity of various hPDI mutants with point mutations on the domain interfaces observed in the compact reduced **bb'xa'** (such as R300A, W396A, K326E, and E431K) to interfere with the ability of conformational transfer. These mutants showed chaperone activity similar to that of the wild-type hPDI in the oxidized form but higher chaperone activity in the presence of DTT (Fig. 6A), indicating that disruption of the interdomain rearrangement can interfere with redox-dependent chaperone activity changes. To further verify the importance of the **a'** domain in

the redox-regulated chaperone activity of hPDI, we finally tested different hPDI truncations. Oxidized **bb'xa'** suppressed the aggregation of GAPDH more efficiently than oxidized **abb'x**, and the presence of DTT decreased the chaperone activity of **bb'xa'** remarkably (Fig. 6B). Because we and others have previously indicated that the four domains of the PDI molecule are all required for binding to large substrates (21, 22), such as the GAPDH folding intermediate (22), chaperone activity of **abb'x** still showed some, but much less, redox regulation (Fig. 6B). Taken together, all of the above results demonstrated that the conformational transfer, based on interdomain rearrangement and triggered by the active site of the **a'** domain, is essential for the redox-regulated chaperone activity of hPDI.

## DISCUSSION

PDI is a multidomain protein that functions as both a dithiol-disulfide oxidoreductase and a chaperone to promote the oxidative folding or reductive unfolding of various protein substrates. Conformational changes of PDI are indicated to be a key factor for its promiscuous binding nature (24, 25, 43). The results presented here provide structural insights into the molecular mechanism of redox-regulated interdomain conformational changes and chaperone activity of hPDI.

We found that the redox-regulated conformational changes of hPDI are mainly located in the **b'xa'** region and triggered by redox switch of the active site in the **a'** domain. Interestingly, this location is in line with the major flexible region in hPDI revealed by our previous work (25), indicating that the large flexibility in the **b'xa'** region is required for the interdomain conformational change. Furthermore, the redox-regulated conformational change happened only when an active thioredoxin-like domain (either **a** or **a'**) connected to the C termini of **b'x**, clearly demonstrating that the **b'** domain and the **x** linker are the necessary components for the conformational change of hPDI regulated by redox. Hence, the domain organization integrity of **b'xa'** determines its redox-dependent regulation in nature.

The crystal structure of the reduced **bb'xa'**, which is the longest fragment of hPDI with structure determined so far, allowed us to understand the underlying molecular mechanism. Particularly, it is the first time that the **b'xa'** region of hPDI has been observed at the atomic level; this is the most critical region for the versatile activities of hPDI (21, 46–48). The structure revealed a novel domain organization (*i.e.* **a'** domain packs tightly with both the **b'** domain and the **x** linker to form one compact structural module). Previous  $^1\text{H}$ - $^{15}\text{N}$  HSQC spectra comparison of **b'-a'oxi** and **b'-a'red** of PDI from thermophilic fungus showed that the redox states of the **a'** domain influence the dynamic properties of the **b'** domain (34), and the small angle x-ray scattering studies revealed a redox-regulated interdomain motion of the **a'** domain (33). Here we uncovered multiple interactions between the **b'** and **a'** domains in detail according to the reduced **bb'xa'** structure. We further identified the regions and residues exposed upon the oxidation of the **a'** domain by mass spectrometry analysis, which were reversely shielded in the reduced form of **bb'xa'**, further demonstrating that the oxidation of the **a'** domain releases the compact structure module.

## Oxidation of hPDI Activates Its Chaperone Activity

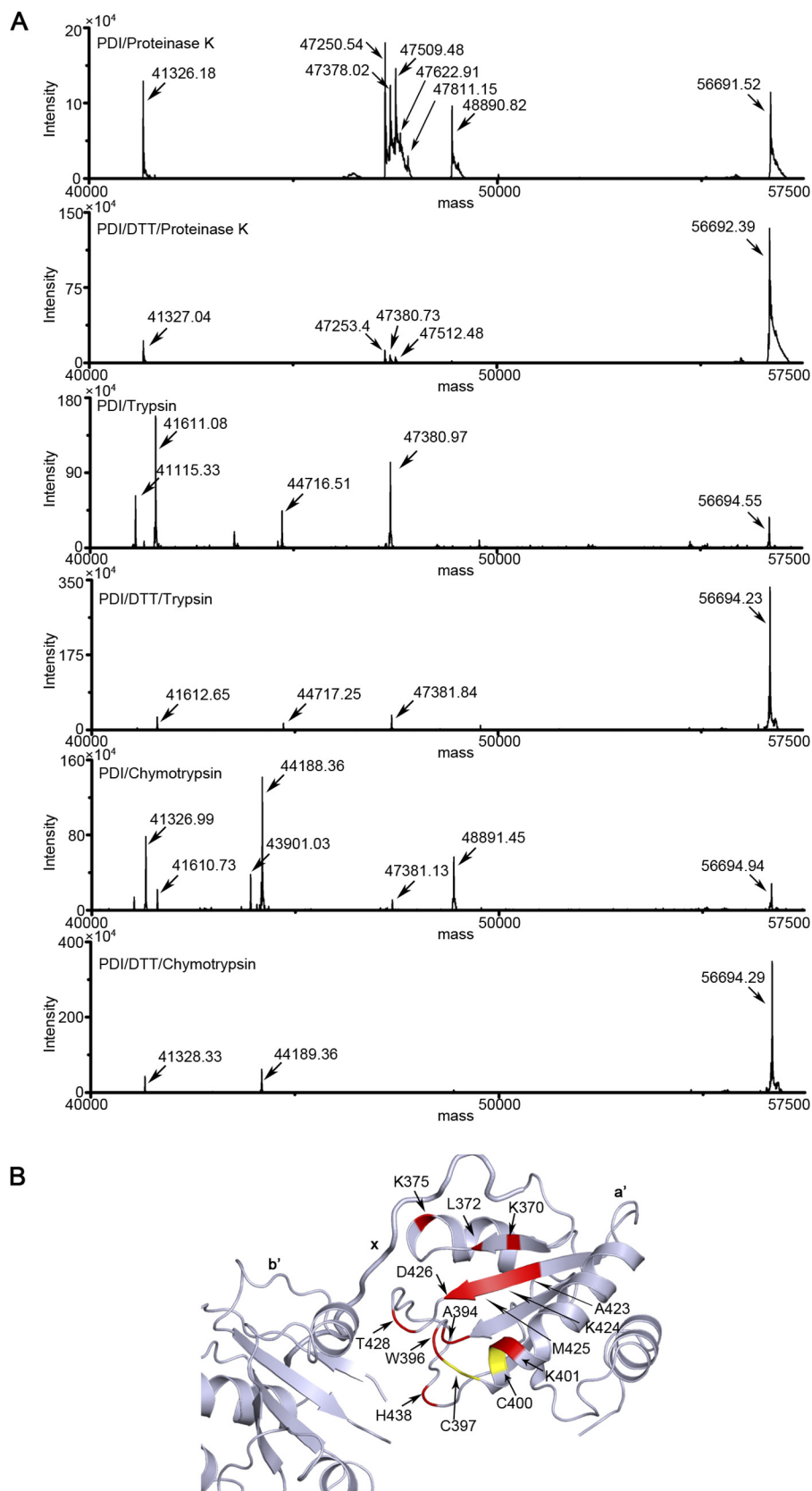
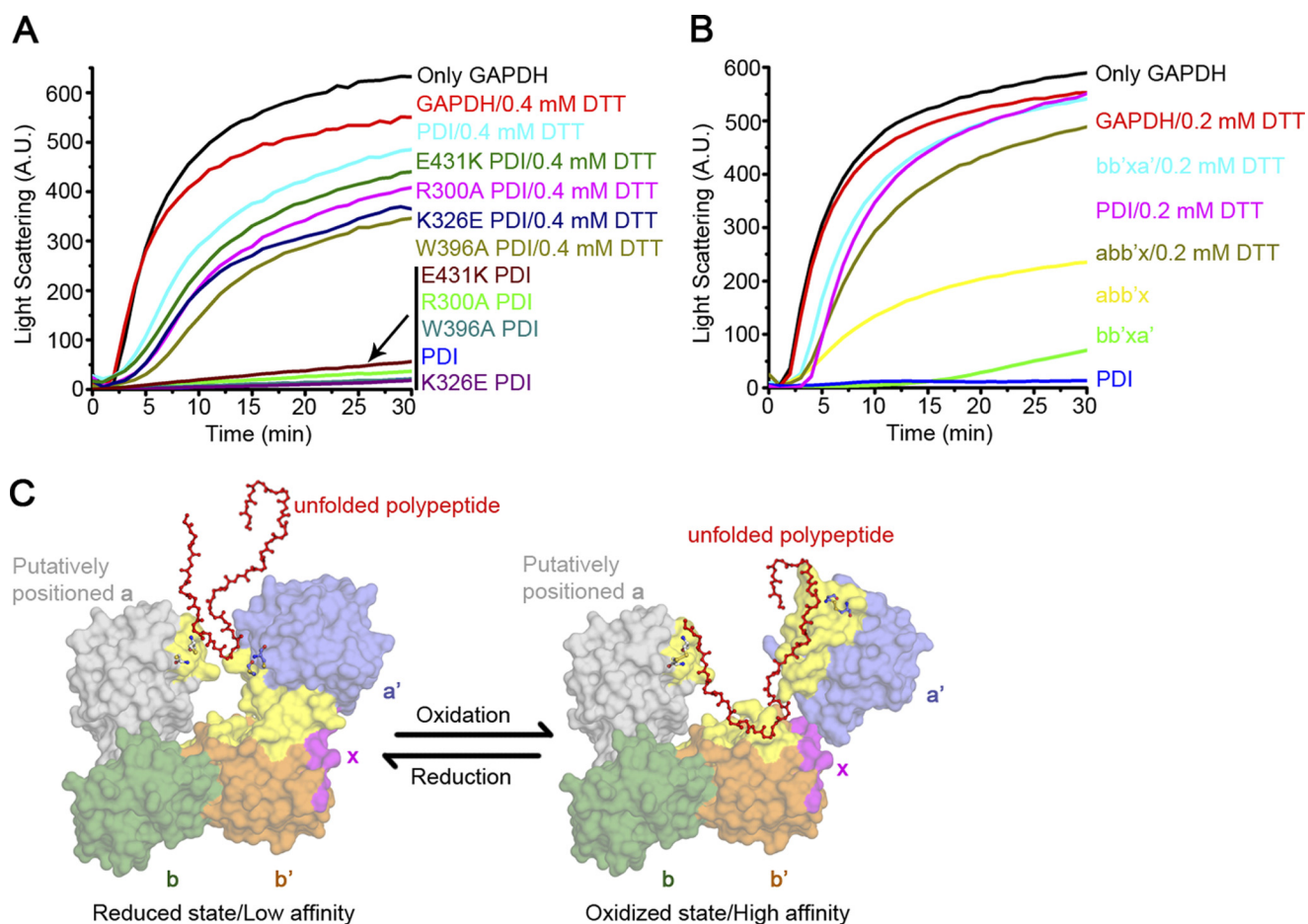


FIGURE 5. **Oxidation of the a' domain release the compact structure formed by domains b', a' and the x linker.** *A*, mass spectrum of the digestion products of hPDI at different redox states. hPDI at 1 mg/ml was incubated with or without 1 mM DTT at 25 °C for 30 min and then digested by 0.3  $\mu$ g/ml proteinase K, 2  $\mu$ g/ml trypsin or chymotrypsin for 5 min. The reactions were terminated by adding PMSF to a final concentration of 0.5 mM and analyzed by mass spectrometry. *B*, mapping the identified redox-dependent digestion sites of hPDI onto the three-dimensional structure of **bb'xa'**. The digestions sites are shown in red, and the active sites are shown in yellow.



**FIGURE 6. Redox-regulated chaperone activity of hPDI.** *A* and *B*, guanidine hydrochloride-denatured GAPDH at 0.14 mM was 50-fold diluted into refolding buffer in the absence or presence of 28  $\mu$ M (*A*) or 5.6  $\mu$ M (*B*) hPDI proteins with various concentrations of DTT as indicated. Aggregation produced during the refolding was monitored by recording the light scattering at 488 nm, and the suppression of aggregation was used to measure the chaperone activity of hPDI proteins. *C*, a schematic model of redox-regulated chaperone activity of hPDI. The **b**, **b'**, **x**, and **a'** domains are colored in green, orange, magenta, and blue, respectively. The position of the **a** domain (gray) in this model is achieved by superposition of the **bb'xa'** structure with that of yPDI at 4 °C (23). Residues involved in ligand binding (23, 34, 43, 44) are colored in yellow. Active sites of both the **a** and **a'** domains are shown in stick representations. The reduced hPDI adopts the compact conformation with small hydrophobic areas exposed for substrate binding, and oxidation of the **a'** domain of hPDI results in exposure of more extended hydrophobic areas for its substrate binding and chaperone activity.

How does the redox switch of the **a'** domain active site trigger the large interdomain conformational change? It is found that the residue Trp-396, adjacent to the active site ([supplemental Fig. S3B](#)), interacts with domain **b'** in the reduced state but is exposed upon oxidation of the **a'** domain active site, indicating its important role in sensing the redox change and triggering the redox-regulated interdomain conformational changes. Another region involved in this conformational change is the  $\beta$ 2- $\beta$ 3 loop ([supplemental Fig. S3B](#)), which extensively interacts with domain **b'** in the reduced state and is exposed upon oxidation. In addition, this loop, although far away from the active site in the primary sequence, contains an extremely well conserved (in thioredoxin-like proteins) *cis*-proline (Pro-441) located adjacent to the active site in the three-dimensional structure ([supplemental Fig. S3B](#)) that has been shown to be involved in substrate binding/release based on the studies of thioredoxin (49), DsbA (50), and yPDI (23). Therefore, Pro-441 may also play a critical role in sensing the redox change. Interestingly, both Trp-396 (adjacent to the active site) and His-438 (near the *cis*-proline) were found in alternative conformations in the reduced **bb'xa'** structure ([supplemental Fig. S3B](#)). The high

mobility of these two residues may contribute to sensing redox microenvironment and triggering conformational changes.

The redox-regulated interdomain conformational changes of the **b'** and **a'** domain can be further supported by the flexibility of the **x** linker. It has been reported that the N-terminal part of the **x** linker can stabilize the **b'** domain (18), whereas the C-terminal part loosely interacts with the **a'** domain and does not contribute to its structural integrity (51). Actually, the C-terminal portion of the **x** linker has been reported to adopt multiple conformations (25, 43), which may further increase interdomain mobility of the **b'xa'** region and underpin the redox-regulated conformational changes. Besides PDI, a number of other PDI family members also contain a linker connecting the **b'** and **a'** domains (17), and it is worthwhile to further explore whether such redox-regulated conformational changes exist in these members.

PDI displays its chaperone activity by temporarily binding with unfolded polypeptides/proteins or folding intermediates through hydrophobic interactions, thereby preventing the misfolding and aggregation of substrates (52). ANS fluorescence

## Oxidation of hPDI Activates Its Chaperone Activity

studies showed that the reduced hPDI exposed smaller hydrophobic area. The crystal structure of reduced **bb'xa'** also revealed that several residues in both the **b'** and **a'** domains, supposed to be involved in substrate binding, are shielded in the compact structure and released to be exposed to solvent upon the oxidation of the **a'** domain active site. It is logical to suppose that such prominent conformational changes induced by different redox states may lead to potential regulation of hPDI chaperone activity. Indeed, we showed in this study that the chaperone activity of hPDI in suppressing the aggregation of GAPDH folding intermediates is redox-regulated. A schematic model of redox-regulated chaperone activity of PDI is shown in Fig. 6C.

Previously, PDI was shown as a redox-regulated chaperone to unfold the cholera toxin A1 subunit (29), and **bb'xa'** was shown to be necessary and sufficient to trigger the unfolding (48). Therefore, the redox-regulated conformational changes in the **b'xa'** region identified here may also be involved in this process. In their toxin unfolding assay, the reduced PDI showed higher binding affinity to bind with the folded toxin A1 subunit and then unfold and release it after being oxidized (29), whereas in our GAPDH refolding assay, the oxidized PDI preferentially associates with partially folded GAPDH folding intermediates to facilitate its folding. There are some other cases: the reduced PDI showed higher binding affinities with Ero1-L $\alpha$  (53) and antigen peptides (54), and the oxidized PDI displayed higher affinities with mastoparan (34) and  $\alpha$ -subunit of prolyl-4-hydroxylase (31). These observations suggested that PDI at different redox states may recognize different substrates; however, the general mechanism is still unknown.

A well studied redox-regulated chaperone, Hsp33, is a conserved heat shock protein in prokaryotes (55). Induced by oxidation along with unfolding, the chaperone activity of Hsp33 is activated with exposure of its buried hydrophobic surfaces in the reduced form. Although the redox-regulated activation of chaperone activity of PDI was previously considered distinct from Hsp33 (29, 56), our results showed that it is similar to Hsp33 (*i.e.* oxidation of PDI significantly increases its chaperone activity). This feature thereby may endow PDI with the first characterized redox-regulated chaperone in the ER for sensing and protecting protein damage from reactive oxygen species (consistently generated in the ER (39)), further explaining why PDI plays a critical role in protecting neurodegenerative disease induced by oxidative stress and/or protein misfolding (39).

*Acknowledgments*—We thank Prof. Mingjie Zhang for stimulating discussion and helpful advice on this work, Prof. Fuquan Yang and Dr. Zhensheng Xie for mass spectrometry analysis, Wenqi Li for some preliminary work, and Prof. Paul Curmi for kindly reading the paper.

## REFERENCES

1. Sitia, R., and Braakman, I. (2003) *Nature* **426**, 891–894
2. Goldberger, R. F., Epstein, C. J., and Anfinsen, C. B. (1963) *J. Biol. Chem.* **238**, 628–635
3. Cai, H., Wang, C. C., and Tsou, C. L. (1994) *J. Biol. Chem.* **269**, 24550–24552
4. Wilson, R., Lees, J. F., and Bulleid, N. J. (1998) *J. Biol. Chem.* **273**, 9637–9643
5. Freedman, R. B., Klappa, P., and Ruddock, L. W. (2002) *EMBO Rep.* **3**, 136–140
6. Molinari, M., Galli, C., Piccaluga, V., Pieren, M., and Paganetti, P. (2002) *J. Cell Biol.* **158**, 247–257
7. Lee, S. O., Cho, K., Cho, S., Kim, I., Oh, C., and Ahn, K. (2010) *EMBO J.* **29**, 363–375
8. Pihlajaniemi, T., Helaakoski, T., Tasanen, K., Myllylä, R., Huhtala, M. L., Koivu, J., and Kivirikko, K. I. (1987) *EMBO J.* **6**, 643–649
9. Wetterau, J. R., Combs, K. A., Spinner, S. N., and Joiner, B. J. (1990) *J. Biol. Chem.* **265**, 9800–9807
10. Turano, C., Coppari, S., Altieri, F., and Ferraro, A. (2002) *J. Cell. Physiol.* **193**, 154–163
11. Fenouillet, E., Barbouche, R., and Jones, I. M. (2007) *Antioxid. Redox Signal.* **9**, 1009–1034
12. Essex, D. W. (2009) *Antioxid. Redox Signal.* **11**, 1191–1225
13. Hoffstrom, B. G., Kaplan, A., Letso, R., Schmid, R. S., Turmel, G. J., Lo, D. C., and Stockwell, B. R. (2010) *Nat. Chem. Biol.* **6**, 900–906
14. Uehara, T., Nakamura, T., Yao, D., Shi, Z. Q., Gu, Z., Ma, Y., Masliah, E., Nomura, Y., and Lipton, S. A. (2006) *Nature* **441**, 513–517
15. Walker, A. K., Farg, M. A., Bye, C. R., McLean, C. A., Horne, M. K., and Atkin, J. D. (2010) *Brain* **133**, 105–116
16. Walker, A. K., and Atkin, J. D. (2011) *Neurol. Res. Int.* **2011**, 317340
17. Alanen, H. I., Salo, K. E., Pekkala, M., Siekkinen, H. M., Pirneskoski, A., and Ruddock, L. W. (2003) *Antioxid. Redox Signal.* **5**, 367–374
18. Pirneskoski, A., Klappa, P., Lobell, M., Williamson, R. A., Byrne, L., Alanen, H. I., Salo, K. E., Kivirikko, K. I., Freedman, R. B., and Ruddock, L. W. (2004) *J. Biol. Chem.* **279**, 10374–10381
19. Freedman, R. B., Gane, P. J., Hawkins, H. C., Hlodan, R., McLaughlin, S. H., and Parry, J. W. (1998) *Biol. Chem.* **379**, 321–328
20. Darby, N. J., and Creighton, T. E. (1995) *Biochemistry* **34**, 11725–11735
21. Klappa, P., Ruddock, L. W., Darby, N. J., and Freedman, R. B. (1998) *EMBO J.* **17**, 927–935
22. Sun, X. X., Dai, Y., Liu, H. P., Chen, S. M., and Wang, C. C. (2000) *Biochim. Biophys. Acta* **1481**, 45–54
23. Tian, G., Xiang, S., Noiva, R., Lennarz, W. J., and Schindelin, H. (2006) *Cell* **124**, 61–73
24. Tian, G., Kober, F. X., Lewandrowski, U., Sickmann, A., Lennarz, W. J., and Schindelin, H. (2008) *J. Biol. Chem.* **283**, 33630–33640
25. Wang, C., Chen, S., Wang, X., Wang, L., Wallis, A. K., Freedman, R. B., and Wang, C. C. (2010) *J. Biol. Chem.* **285**, 26788–26797
26. Hatahet, F., and Ruddock, L. W. (2009) *Antioxid. Redox Signal.* **11**, 2807–2850
27. Mezghrani, A., Fassio, A., Benham, A., Simmen, T., Braakman, I., and Sitia, R. (2001) *EMBO J.* **20**, 6288–6296
28. Zito, E., Melo, E. P., Yang, Y., Wahlander, Å., Neubert, T. A., and Ron, D. (2010) *Mol. Cell* **40**, 787–797
29. Tsai, B., Rodighiero, C., Lencer, W. I., and Rapoport, T. A. (2001) *Cell* **104**, 937–948
30. Tsai, B., and Rapoport, T. A. (2002) *J. Cell Biol.* **159**, 207–216
31. Lumb, R. A., and Bulleid, N. J. (2002) *EMBO J.* **21**, 6763–6770
32. Winter, J., and Jakob, U. (2004) *Crit. Rev. Biochem. Mol. Biol.* **39**, 297–317
33. Nakasako, M., Maeno, A., Kurimoto, E., Harada, T., Yamaguchi, Y., Oka, T., Takayama, Y., Iwata, A., and Kato, K. (2010) *Biochemistry* **49**, 6953–6962
34. Serve, O., Kamiya, Y., Maeno, A., Nakano, M., Murakami, C., Sasakawa, H., Yamaguchi, Y., Harada, T., Kurimoto, E., Yagi-Utsumi, M., Iguchi, T., Inaba, K., Kikuchi, J., Asami, O., Kajino, T., Oka, T., Nakasako, M., and Kato, K. (2010) *J. Mol. Biol.* **396**, 361–374
35. Li, S. J., Hong, X. G., Shi, Y. Y., Li, H., and Wang, C. C. (2006) *J. Biol. Chem.* **281**, 6581–6588
36. Otwinowski, Z., and Minor, W. (1997) *Methods Enzymol.* **276**, 307–326
37. Murshudov, G. N., Vagin, A. A., and Dodson, E. J. (1997) *Acta Crystallogr. D Biol. Crystallogr.* **53**, 240–255
38. Emsley, P., and Cowtan, K. (2004) *Acta Crystallogr. D Biol. Crystallogr.* **60**, 2126–2132
39. Malhotra, J. D., and Kaufman, R. J. (2007) *Antioxid. Redox Signal.* **9**, 2277–2293
40. Brünger, A. T., Adams, P. D., Clore, G. M., DeLano, W. L., Gros, P.,

- Grosse-Kunstleve, R. W., Jiang, J. S., Kuszewski, J., Nilges, M., Pannu, N. S., Read, R. J., Rice, L. M., Simonson, T., and Warren, G. L. (1998) *Acta Crystallogr. D Biol. Crystallogr.* **54**, 905–921
41. Painter, J., and Merritt, E. A. (2006) *Acta Crystallogr. D* **62**, 439–450
  42. Laskowski, R. A., Moss, D. S., and Thornton, J. M. (1993) *J. Mol. Biol.* **231**, 1049–1067
  43. Nguyen, V. D., Wallis, K., Howard, M. J., Haapalainen, A. M., Salo, K. E., Saaranen, M. J., Sidhu, A., Wierenga, R. K., Freedman, R. B., Ruddock, L. W., and Williamson, R. A. (2008) *J. Mol. Biol.* **383**, 1144–1155
  44. Denisov, A. Y., Määttänen, P., Dabrowski, C., Kozlov, G., Thomas, D. Y., and Gehring, K. (2009) *FEBS J.* **276**, 1440–1449
  45. Dong, G., Wearsch, P. A., Peaper, D. R., Cresswell, P., and Reinisch, K. M. (2009) *Immunity* **30**, 21–32
  46. Pirneskoski, A., Ruddock, L. W., Klappa, P., Freedman, R. B., Kivirikko, K. I., and Koivunen, P. (2001) *J. Biol. Chem.* **276**, 11287–11293
  47. Wang, L., Li, S. J., Sidhu, A., Zhu, L., Liang, Y., Freedman, R. B., and Wang, C. C. (2009) *J. Biol. Chem.* **284**, 199–206
  48. Forster, M. L., Mahn, J. J., and Tsai, B. (2009) *J. Biol. Chem.* **284**, 13045–13056
  49. Maeda, K., Häggglund, P., Finnie, C., Svensson, B., and Henriksen, A. (2006) *Structure* **14**, 1701–1710
  50. Kadokura, H., Tian, H., Zander, T., Bardwell, J. C., and Beckwith, J. (2004) *Science* **303**, 534–537
  51. Kozlov, G., Määttänen, P., Thomas, D. Y., and Gehring, K. (2010) *FEBS J.* **277**, 3924–3936
  52. Wilkinson, B., and Gilbert, H. F. (2004) *Biochim. Biophys. Acta* **1699**, 35–44
  53. Masui, S., Vavassori, S., Fagioli, C., Sitia, R., and Inaba, K. (2011) *J. Biol. Chem.* **286**, 16261–16271
  54. Cho, K., Cho, S., Lee, S. O., Oh, C., Kang, K., Ryoo, J., Lee, S., Kang, S., and Ahn, K. (2011) *Antioxid. Redox Signal.* **15**, 621–633
  55. Kumsta, C., and Jakob, U. (2009) *Biochemistry* **48**, 4666–4676
  56. Sitia, R., and Molteni, S. N. (2004) *Sci. STKE* 2004, pe27